Journal Pre-proof

Hydrophobicity gradient optimization of fuel cell gas diffusion media for its application in vehicles

Qinwen Yang , Zhen Zhang , Gang Xiao , Deyi Xue

PII: S2667-3258(24)00027-X
DOI: https://doi.org/10.1016/j.fmre.2024.01.007
Reference: FMRE 704

To appear in: *Fundamental Research*

Received date: 9 April 2023
Revised date: 10 January 2024
Accepted date: 16 January 2024

Please cite this article as: Qinwen Yang , Zhen Zhang , Gang Xiao , Deyi Xue , Hydrophobicity gradient optimization of fuel cell gas diffusion media for its application in vehicles, *Fundamental Research* (2024), doi: https://doi.org/10.1016/j.fmre.2024.01.007

Hydrophobicity gradient optimization of fuel cell gas diffusion media for its application in vehicles

Qinwen Yang[1], Zhen Zhang[1], Gang Xiao[2*], Deyi Xue[3]

1 College of Mechanical and Vehicle Engineering, State Key Laboratory of Advanced Design and Manufacturing for Vehicle Body, Hunan University, Changsha 410082, China

2 School of Mechanical and Electrical Engineering, Central South University, Changsha 410083, China

3 Department of Mechanical and Manufacturing Engineering, University of Calgary, Calgary, Alberta, Canada T2N 1N4

Abstract

During Fuel Cell Vehicle (FCV) operation, the liquid water in gas diffusion media (GDM) prevents the reaction gas from reaching the reaction zone and lead to output power fluctuation and reduce the lifespan of FCV. In the present research, hydrophobicity gradient settings of micro-porous layer (MPL) and gas diffusion layer (GDL) are optimized to improve the water removal ability of GDM. Computational fluid dynamics (CFD) model is constructed for numerical simulations to analyze the fuel cell power output and the water content in the GDM with different hydrophobicity gradients. Experiments with different hydrophobicity gradients, which are specifically prepared with corresponding concentrations of polytetrafluoroethylene (PTFE) solutions, are conducted for validation of simulation results. It is shown that the positive hydrophobicity gradient of MPL and GDL provides a better capacity for water removal and oxygen transport. The contact angles of MPL and GDL are further optimized as 147.9°-138.6° by genetic algorithm integrated with the CFD simulations.

Keywords: PEMFC; hydrophobicity gradient; water management; fuel cell vehicle; optimization

* E-mail address: Xgang1221@163.com (Dr. Gang Xiao)

1 Introduction

A Fuel Cell Vehicle (FCV) is powered by polymer electrolyte membrane fuel cells (PEMFCs) which consumes hydrogen and oxygen with the advantages of high efficiency, zero pollution, low temperature, and quiet operation. Because of these advantages, FCVs have been studied and promoted by many countries for green transportation. However, the durability and stability of fuel cells, which are significantly influenced by the water management[1],[2], still need to be improved for commercialization of FCVs. Better water management can ensure output power stability and enhance the lifespans of components, thus reducing the operating costs and accelerating the commercialization process[3],[4]. The Nafion membrane should be well hydrated during operation. It is indicated that the appropriate water content should be maintained in the PEMFC. Meanwhile, the flooding of PEMFC will make it difficult for the reaction gas to reach the reaction zone, resulting in a sudden voltage drop and even voltage reversal. In the case of voltage reversal, significant heat is generated to damage the PEMFC structure, such as the perforation of the membrane and bipolar plate. Under that condition, it will reduce the service life of PEMFC and lead to a serious safety risk due to the mixing of hydrogen and air[5-9]. Water management plays a significant role for output performance and safety of FCV.

To improve water management in FCVs, many studies have been carried out on the optimization of the PEMFC parameters[10]. The gas diffusion media (GDM) has a great influence on water management and is widely considered for PEMFC performance improvement[11]. The GDM includes micro-porous layer (MPL) and gas diffusion layer (GDL), which are mass transport media with the function of supporting and stabilizing the electrode structures. Some research teams focused on PEMFC performance affected by the hydrophobicity gradient which could be represented by the contact angles between the micro-porous layer (MPL) and gas diffusion layer (GDL). The contact angle is the angle at which a liquid interface meets a solid surface. A high contact angle indicates hydrophobicity (water-repelling), while a low contact angle indicates hydrophilicity (water-attracting). The different contact

angles of MPL and GDL form the different hydrophobicity gradients (i.e., the changes of hydrophilicity between MPL and GDL). In application, use of the polytetrafluoroethylene (PTFE) loading on GDM is a traditional method to get different contact angles[12]. Weng et al. [13] compared the PEMFC performance with different hydrophobicity gradients which used different concentrations of PTFE solutions to treat MPL and GDL. It was concluded that the inverse hydrophobicity gradient could help keep water under low relative humidity (RH) and high PTFE loading should be avoided. Liu et al. [14] focused on different contact angles of GDL and compared the PEMFC performances at different RH measures. The results showed that the performance differences with various contact angles under different RH measures were mainly caused by water retention ability and pore structure which were influenced by PTFE treatment. Wang et al. [15] used different materials to form different gradients to investigate the influence of hydrophobicity gradient on PEMFC performance. In their study, electrochemical impedance spectra (EIS) was used to explain the performance differences. Naito et al. [16] focused on the influence of carbon paper thicknesses and hydrophobicity gradients on water behaviors. Chun et al. [17] used double MPL with different hydrophobicity gradients to make membrane electrode assemblies (MEAs) and compare them with single MPL MEA. In their work, they called a smaller contact angle as hydrophilic even though it was higher than 90°. Hou et al. [18] produced a self-humidifying MEA by inserting a layer of hydrophilic T_iO_2 and testing under low RH. Tanuma et al. [19] focused on the influence of GDL on water behavior by making MEA that the anode and cathode were assembled with different GDLs, respectively.

As PTFE is widely used to treat the GDL and MPL to form different hydrophobicity gradients, the material characteristics of GDL and MPL affected by PTFE loads have been studied by many researchers. Ismail et al. [20] investigated the electrical conductivity of GDL with different PTFE loads. Reshetenko et al. [21] used scanning electron microscopy (SEM) and mercury intrusion porosimetry (MIP) to study the effect of PTFE loading in GDL particularly. The HNEI segmented cell system was utilized to obtain the polarization curve and implement the EIS and cyclic

voltammetry (CV) test to investigate the effect of different PTFE loadings in GDL on MEA. Hwang et al. [22] focused on the porosity change of GDL with different PTFE loadings. In their work, the experimental data were used to fit the effective diffusivity which was affected by porosity. Jinuntuya et al. [23] investigated the breakthrough pressure, water flow rate, and water retention in the GDL with different PTFE loadings. Kuwertz et al. [24] implemented the experiment to get the porosity, pore volume, contact angle, pore diameter, and impedance through different PTFE loadings of GDL.

Numerical simulations have been widely used for the water management of PEMFC as they are efficient and easy to observe, compared to experiments. Some researchers applied machine learning in PEMFC optimization[25]. Wang et al. [26] built a sophisticated M^5 model with integrated physics-based simulation and machine-learning-based surrogate modeling for the GDL optimization. Some researchers established the CFD models for the PEMFC to predict the performance and analyze the distributions of reactants and products. Zhang et al. [27] established a two-fluid model to investigate the effect of channel shape on the distribution of liquid water. Arif et al. [28] studied the influence of porosity and contact angle on water content and PEMFC performance, respectively. Several research works used the volume of fluid (VOF) method to simulate the air-water two-phase flow in the PEMFC gas channel and focused on the liquid drop behaviors on different surfaces. Chen et al. [29] studied the water transport and morphology changes in the gas channel under different airflow velocity and water injection velocity conditions. Ferreira et al. [30] combined the 1D and VOF methods to simulate the water produced in GDL and transport in the gas channel with different operation conditions. Some researchers combined the Lattice Boltzmann Method (LBM) and 3D reconstruction to simulate the liquid water movement in the GDL[31-35].

However, in the simulation work of hydrophobicity gradient design and water management in PEMFC, only the influence of contact angles has been considered. The porosity change caused by the PTFE solution and the influence of porosity on water management were ignored. To better improve the water management for the

PEMFC, it is necessary to study the effect of hydrophobicity gradient on PEMFC considering the porosity factor.

In this study, both the porosity and the contact angle which are influenced by PTFE are considered in the design of the hydrophobicity gradient. The water removal capacity of GDM is further discussed for PEMFC performance improvement. A numerical model for a 5-cell stack is constructed for simulation to better understand the mechanisms on the performance differences with different contact angles. The EIS test is then conducted with our customized MEA for validation. The Eulerian model is used to simulate the water drop behavior in GDM with different hydrophobicity gradients. Furthermore, CFD models are integrated with optimization methods to optimize the contact angles of MPL and GDL which are used to represent the hydrophobicity gradient.

2 Modeling and Experiment

2.1 Computational domain

In this study, a 5-cell stack model is constructed to represent the PEMFC engine for analyses. This model is composed of different components of the PEM and BPs (bipolar plates), GCs (gas channels), GDLs, MPLs, and CLs (catalyst layers). The computational domain of the 5-cell stack model is shown in Figure 1. The MEA includes PEM and the GDLs, MPLs, and CLs of the anode and cathode. A GC consists of seven serpentine channels which are connected by the manifold. The length of a single serpentine channel is 140 mm and the cross-section size is 1 mm × 1 mm. The geometric parameters for both the anode and the cathode are completely same. The geometric parameters of the 5-cell stack model are shown in Table 1.

Table 1. Geometric parameters of the 5-cell stack model

Parameters	Value
MEA area (cm^2)	51.6
Rib width (mm)	1
Channel width (mm)	1
Channel height (mm)	1
Channel number (serpentine)	21

Length (PEM, CL, MPL, GDL, BP) (mm)	120
Width (PEM, CL, MPL, GDL, BP) (mm)	43
Thickness (PEM, CL, MPL, GDL) (mm)	0.0255, 0.01, 0.02, 0.1

The model for simulating the droplet diffusion in GDM with different hydrophobicity gradients is shown in Figure 2. In the droplet diffusion model, the MPL and GDL are separated from PEMFC to investigate the water behaviors between the MPL and GDL. The parameters of MPL and GDL are the same as PEMFC. The model mainly includes patch area, MPL, and GDL. The patch area is a space with the same parameters as the MPL and is used to generate the droplet in the simulation.

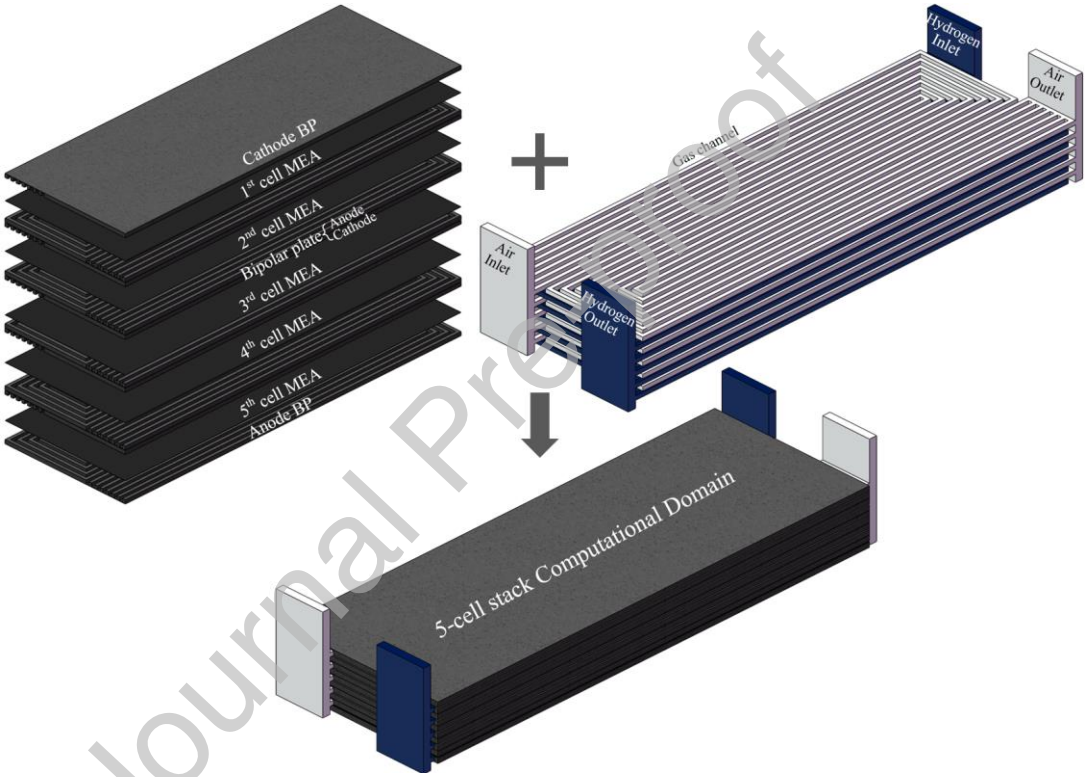

Figure. 1. Computational domain of the 5-cell stack model

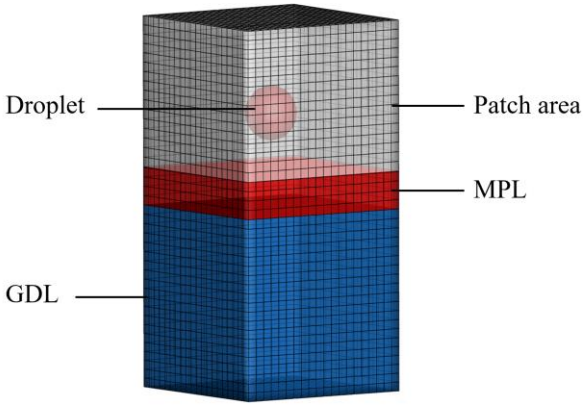

Figure. 2. Droplet diffusion model

2.2 Simulation conditions

Based on the ANSYS PEM fuel cell module, a 3D model is used to study the performance and species distribution of the PEMFC. In this model, the reactions of the anode and cathode are driven by the difference between the phase potential of the solid and the phase potential of the electrolyte. The two potential equations of solid and electrolyte are as follows:

$$\nabla \cdot (\sigma_i \nabla \phi_i) + R_i = 0 \tag{1}$$

where σ_i is electrical conductivity of solid or electrolyte, ϕ_i is electric potential, R_i is the volumetric transfer current, which is calculated by Eq (2) and Eq (3):

Anode: $$R_{an} = \left(\zeta_{an} j_{an}(T)\right)\left(\frac{[H_2]}{[H_2]_{ref}}\right)^{\gamma_{an}} \left(e^{\alpha_{an}^{an} F\eta_{an}/RT} - e^{-\alpha_{cat}^{an} F\eta_{an}/RT}\right) \tag{2}$$

Cathode: $$R_{cat} = \left(\zeta_{cat} j_{cat}(T)\right)\left(\frac{[O_2]}{[O_2]_{ref}}\right)^{\gamma_{cat}} \left(-e^{\alpha_{an}^{cat} F\eta_{cat}/RT} + e^{-\alpha_{cat}^{cat} F\eta_{cat}/RT}\right) \tag{3}$$

where $j_{an}(T)$ and $j_{cat}(T)$ are reference exchange current densities of anode and cathode, ζ_{an} and ζ_{cat} are specific active surface areas of anode and cathode, $[H_2]$ and $[H_2]_{ref}$ are local concentration and reference values of hydrogen, $[O_2]$ and $[O_2]_{ref}$ are local concentration and reference values of oxygen, α_{an}^{an} and α_{cat}^{an} are anode and cathode transfer coefficients of the anode electrode, α_{an}^{cat} and α_{cat}^{cat} are anode and cathode transfer coefficients of the cathode electrode, F is the Faraday constant, R is the universal gas constant, T is temperature, and η_i is surface overpotential calculated by Eq (4):

$$\eta_i = \phi_{sol} - \phi_{mem} - U_i^0 \tag{4}$$

U_i^0 is the potential at anode or cathode calculated by Eq (5) or Eq (6):

$$U_{an}^0 = E_{an}^0 - \frac{\Delta S_{an}}{2F}(T - T^0) - \frac{RT}{2F}\ln\left(\frac{P_{H_2}}{P^0}\right) \tag{5}$$

$$U_{cat}^0 = E_{cat}^0 + \frac{\Delta S_{cat}}{2F}(T - T^0) - \frac{RT}{2F} ln\left(\frac{P_{H_2O}}{P_{sat}\sqrt{P_{O_2}/P^0}}\right) \tag{6}$$

where P_{sat} is the water saturation pressure, P_{H_2}, P_{O_2} and P_{H_2O} are the partial pressures of hydrogen, oxygen, and water vapor, E_i^0 is the reversible potential, ΔS_i is the reaction entropies, and T^0 and P^0 are the reference temperature and pressure.

The water transport in the porous and the membrane is described by the Eq (7):

$$\frac{\partial}{\partial t}(\rho_l \varepsilon_i s) = \nabla \cdot \left(\rho_l \frac{KK_r}{\mu_l} \nabla(P_{cap} + P_g)\right) + S_{gl} - S_{ld} \quad (7)$$

where ρ_l is the density of liquid water, ε_i is porosity of porous media, s is liquid saturation, K and K_r are absolute permeability and relative permeability, μ_l is liquid dynamic viscosity, S_{gl} is rate of mass change between gas and liquid phases, S_{ld} is rate of mass change between liquid and dissolved phases, P_g is the pressure of gas, and P_{cap} is the capillary pressure.

In the PEMFC, the driving force of water diffusion in GDM is capillary pressure which is calculated by the Leverett J-function defined as[30]:

$$P_{cap(s)} = \sigma|\cos\theta|\sqrt{\frac{\varepsilon}{K}}J(s) \quad (8)$$

where σ, θ, ε, and K represent the surface tension of water, contact angle, porosity, and intrinsic permeability of GDM respectively. $J(s)$ is calculated by Eq (9), where s is the liquid saturation:

$$J(s) = \begin{cases} 1.417(1-s) - 2.120(1-s)^2 + 1.263(1-s)^3, for\ \theta \le 90^\circ \\ 1.417s - 2.120s^2 + 1.263s^3, for\ \theta > 90^\circ \end{cases} \quad (9)$$

As mentioned before, the contact angle and porosity of GDM are affected by PTFE loading. Eq(10) is utilized for polynomial fitting with the discrete data from Kuwertz et al. [24] to obtain the continuous relationship between contact angle and PTFE content:

$$x = a_0 + a_1\theta^1 + a_2\theta^2 + a_3\theta^3 + a_4\theta^4 \quad (10)$$

where x is the weight fraction of the PTFE, θ is the contact angle, and a_i are the coefficients of polynomial. The values of a_i are -1.901×10^{-6}, 9.542×10^{-4}, -0.172, 13.391, and -373.899 respectively.

With the porosity being affected by PTFE loading, the porosity of GDM is modified with Eq (11) from Reshetenko et al. [21]:

$$\varepsilon = \varepsilon_0 - \frac{V_{PTFE}}{V_{CP}} = \varepsilon_0 - \frac{x}{1-x} \cdot \frac{\rho_{CP}}{\rho_{PTFE}} \quad (11)$$

where ε is the porosity of treated GDM, ε_0 is the porosity of untreated GDL, x is the weight fraction of the PTFE which can be calculated by Eq (10), ρ_{cp} is the density of the carbon paper with value of 0.36 g cm^{-3}, and ρ_{PTFE} is the density of PTFE with the value of 2.15 g cm^{-3}.

Assuming that the PEMFC operates at a steady state, the gas and liquid water flows in the PEMFC are laminar. The contact angle, porosity, and pore size of GDM are homogenous. The porosity parameters for GDL and MPL are set as 0.6 and 0.5. In the simulation, the back pressure of the cathode and anode is 50 kPa, and the RH of inlet gas is 50%. The gas mass flow parameters of the cathode and anode are 5.490×10^{-4} kg s^{-1} and 3.005×10^{-5} kg s^{-1} respectively. Since the output voltage of PEMFC is about 0.6-0.7V under normal operating conditions[36], 0.65V is selected for the single cell voltage. At the endplate of the cathode, a constant voltage is specified.

The contact angles of 95° and 120° are selected to form different hydrophobicity gradients based on the previous research[28-38]. The porosity is calculated by Eq (10) and Eq (11). The positive, inverse, and uniform hydrophobicity gradients are investigated through simulations. The parameters of the different hydrophobicity gradients are shown in Table 2. The operation conditions and model parameters, such as temperature, electric conductivity, and permeability in porous media, are the same for three hydrophobicity gradients with the details listed in Table 3.

Before the simulation, different sets of grid layers are applied along the thickness and in-plane directions to the 5-cell stack and the droplet diffusion model. This operation is utilized to analyze considering grid-independency. With the consideration of both accuracy and efficiency, 23.85 million computational cells are employed for the 5-cell stack model and 16×10^{3} computational cells are employed for the droplet diffusion model.

Table 2. Parameters of the different hydrophobicity gradients in the simulation

Hydrophobicity gradient	Parameters of MPL		Parameters of GDL	
	Contact angle (°)	Porosity	Contact angle (°)	Porosity
Inverse	95	0.471	120	0.565
Positive	120	0.465	95	0.571
Uniform	120	0.465	120	0.565

Table 3. Operation conditions and model parameters

Parameter	value
Electric conductivity (CL, MPL, GDL, BP) (S m^{-1})	5000, 5000, 5000, 20000
Thermal conductivity (CL, MPL, GDL, BP) (W m^{-1} K^{-1})	1.0, 1.0, 0.95, 20

Heat specific capacity (CL, MPL, GDL, membrane) (J kg^{-1} K^{-1})	568, 3300, 3300, 1580
Permeability (CL, GDL, MPL, membrane) (m^2)	2.0×10^{-12}, 1.0×10^{-12}, 1.0×10^{-12}, 2.0×10^{-12}
Exchange current density (A m^{-2})	Anode: 10; Cathode: 1.5×10^{-5}
Transfer coefficient	Anode: 0.5; Cathode: 0.5
Temperature (K)	353.15
Back pressure (kPa)	50

2.3 Experiment

During the simulation, we focus on the contact angle of the cathode as the water is mainly generated at the cathode side. To verify the simulation results, the EIS test has been carried out to investigate cathode mass transfer with different hydrophobicity gradients. The low frequency of the EIS result reflects the water content and oxygen transportation in the MPL and GDL[40]-[44]. Based on the characteristics of the material[21],[24], we treat GDL and MPL with 5% and 20% PTFE solutions to correspond to the different hydrophobicity gradients in simulations. The GDL and MPL treated by PTFE are assembled into the cathode of MEA. The details and the corresponding hydrophobicity gradients of the MEA are shown in Table 4.

The diagram of the experimental system is shown in Figure 3. In the experiment, compressed air and pure hydrogen are supplied to the cathode and anode, respectively. Greenlight G60 is used to sample the experimental data and control the operating parameters of PEMFC, such as current density, gas flow, temperature, back pressure, and the humidity of inlet gas. For the EIS test, the GAMRY is used to generate the alternating current excitation that is superimposed on the load current and sample the data. The setting parameters of GAMRY are controlled by G60, and the data sampled by GAMRY are sent to the G60.

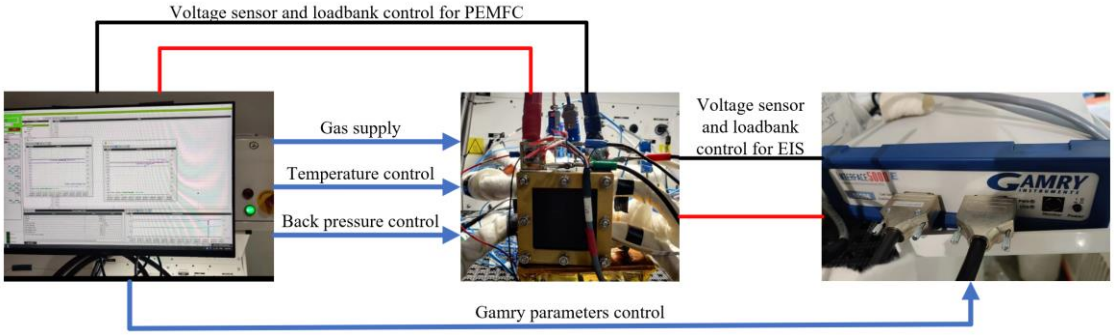

Figure. 3. Diagram of experimental system

During the experiment, the stoichiometry values at the anode and cathode are set to 1.5 and 2.5, respectively. The temperature of PEMFC is set at 80℃, and the back pressure is 50 kPa for both anode and cathode. In the EIS test, the AC excitation current is assigned to 5% of the DC, and the measurement frequency range is 0.1Hz-10kHz. The inlet gas RHs are selected as 30%, 50%, and 100% for each EIS test. The first EIS test and the second EIS test are implemented at the current densities of 2 A cm^{-2} and 1 A cm^{-2}, respectively. Before the EIS test, PEMFC is kept working at the corresponding current density for at least 10 minutes.

Table 4. Hydrophobicity gradient and PTFE content of MPL and GDL at cathode

Group	PTFE content of MPL (%)	PTFE content of GDL (%)	Hydrophobicity gradient
MEA1	5	20	Inverse
MEA2	20	5	Positive
MEA3	20	20	Uniform

3 Results and discussions

3.1 Simulated performance

In the present research, positive, inverse, and uniform hydrophobicity gradients are defined to represent the combinations of MPL and GDL with the contact angles of 120°-95°, 95°-120°, and 120°-120°. Figure 4 shows the comparison of simulation results with the different hydrophobicity gradients of GDM. Since the single cell voltage is set to a constant of 0.65V in the simulation, the current density is used to evaluate the PEMFC performance. The positive hydrophobicity gradient brings a better performance, which is 2.97% higher than the inverse hydrophobicity gradient and 3.09% higher than the uniform hydrophobicity gradient on average. The results may indicate that the positive hydrophobicity gradient has a better capacity for water removal and oxygen transport.

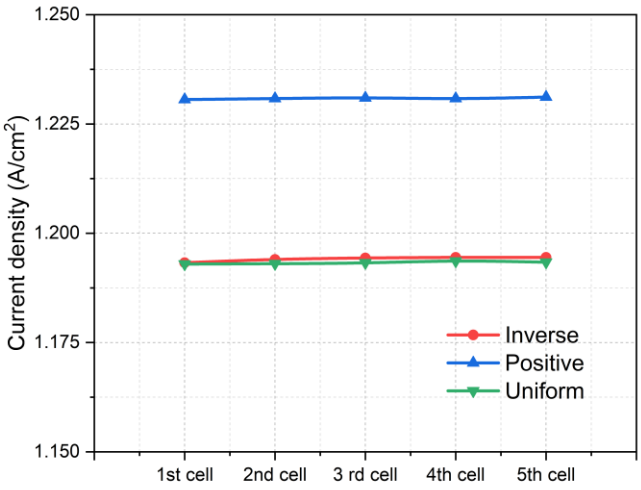

Figure. 4. Comparison among the simulation results

3.2 Water contents in GDM

To understand the reason for the performance variation with different gradients, the water contents in GDM are compared to investigate the working mechanisms. Before analyzing the water content, we should realize that more water is produced in PEMFC and drained out through the GDM at a higher current density. Figure 5 shows the water contents in MPL and GDL. The highest water content is related to the highest current density for the positive gradient type. As for the inverse and uniform gradients, we notice that they have almost the same current density values. However, the water contents of MPL and GDL in the inverse gradient are 1.11% and 0.12% higher than those with the uniform gradient, which indicates that the inverse gradient has a weak water removal ability. We speculate that the inverse hydrophobicity gradient may lead water transport from MPL to GDL harder, which makes water retained in the MPL and hinder oxygen transport.

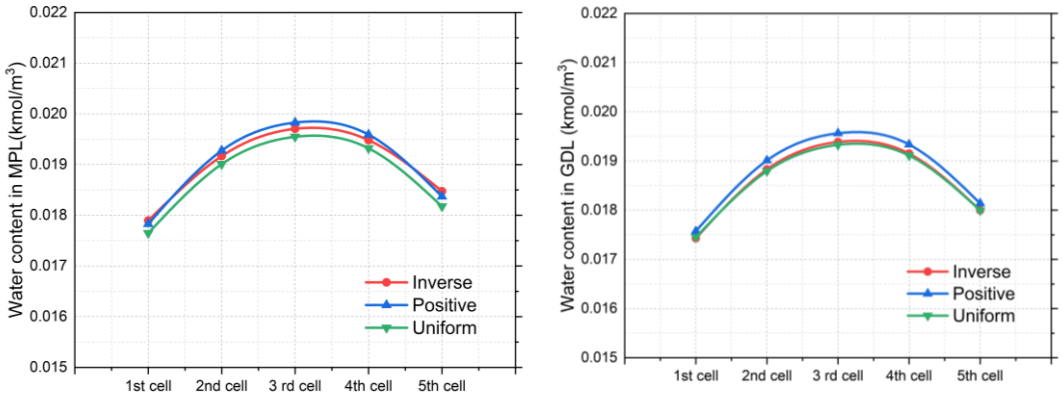

(a) (b)

Figure. 5. Water contents: (a) in cathode MPL; (b) in cathode GDL.

To better understand the fluence of hydrophobicity gradient on water transport, the Eulerian model is used for transient simulation with water droplet diffusion between different hydrophobicity gradients. Figure 6 shows the variation of droplet diffusion in MPL and GDL with time under inverse and positive hydrophobicity gradients, where ms represents milliseconds. Figure 6(a) shows the droplet diffusion in the inverse hydrophobicity gradient. The droplet is generated at relatively hydrophilic media and diffuses with gravity and capillary pressure. At the beginning, the droplet is not spread around. At 2 ms, the droplet reaches the interface of GDM and the main body of the droplet stays at the interface for the rest of the time. Figure 6(b) shows the droplet in the positive hydrophobicity gradient. Different from Figure 6(a), the droplet tends to spread around at 1 ms and the diffusion velocity is higher, the droplet passes through the interface at 2 ms without hinder and keeps diffusing. The main body of the droplet approaches the bottom of GDM at 4 ms and reaches the bottom at 5 ms.

The different water behaviors at the interface between MPL and GDL are identified by comparing the droplet diffusion activities under different hydrophobicity gradients. In the inverse hydrophobicity gradient GDM, the droplet is hindered by the interface and hard to pass through. But in the positive hydrophobicity gradient, the droplet is easy to pass through the interface. Medium 1 and Medium 2 are used to represent the porous media with the contact angles of 95° and 120°, respectively. The

reason for the difference in water behavior may be that Medium 1 has a better water retention capacity while Medium 2 has a better water removal ability. Based on Figure 6(a) at 2 ms, when the water transport from Medium 1 to Medium 2 and reaches the interface of two porous media, the water may get a repulsive force from Medium 2. If the direction of water transport is reversed, the water may be dragged into Medium 1, since Medium 1 has a better wettability, shown in Figure 6 (b) at 2 ms. Meanwhile, the porosity gradient of MPL and GDL in the positive gradient is slightly higher than that in the inverse gradient, which indicates more space in GDL could absorb the liquid water in MPL and be helpful for water removal. This may be another reason for the difference of droplet at the interface. Based on the above analysis, it can be concluded that the positive hydrophobicity gradient in GDM helps to remove the water generated by PEMFC and avoid flooding.

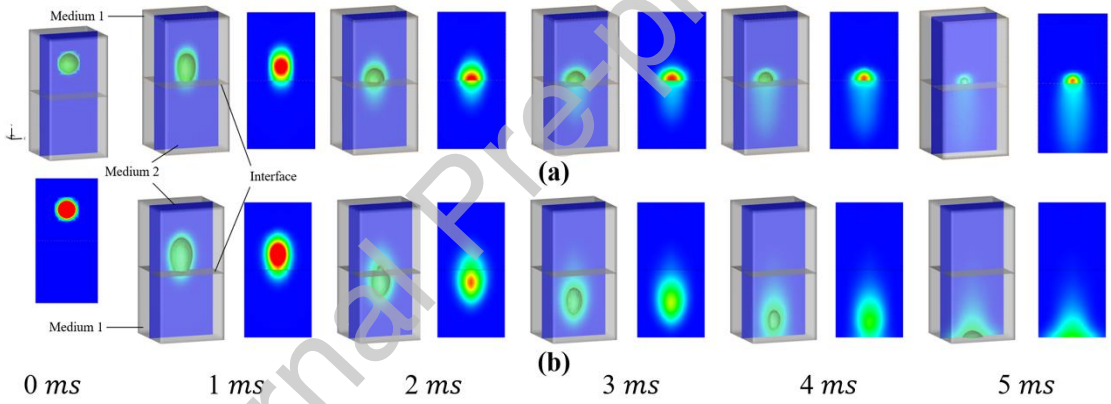

Figure. 6. The diffusion of the droplet in MPL and GDL with time under inverse and positive hydrophobicity gradient conditions: (a) in inverse hydrophobicity gradient GDM; (b) in positive hydrophobicity gradient GDM.

3.3 Oxygen contents in GDM

Figure 7 shows the oxygen contents of MPL and GDL in PEMFC. The positive gradient has a lower oxygen content as it brings a higher current density and consumes more oxygen. As for the inverse and uniform gradients with a similar current density, the oxygen contents of MPL and GDL in the inverse gradient are 6.31% and 3.32%, lower than those with the uniform gradient. It indicates that oxygen transport has been hindered in the inverse gradient since the MPL of inverse has a

better water retention capacity which forms a water film on the GDL-MPL interface and hinders the oxygen transportation from GDL to MPL. The porosity of GDM decreasing from the GC to the CL will enhance the water removal ability[45]. From Table 2, the porosity gradient of the inverse gradient is the lowest among the three hydrophobicity gradients, which further weakens the water removal ability of GDM, makes liquid water occupy the pores, and reduces the oxygen transport capacity of GDM. Based on the analysis results given in Section 3.2 and the oxygen contents of the inverse gradient, it can be concluded that the inverse gradient of GDM will make the water retained in GDM and hinder the oxygen transport from the gas channel to the reaction zone.

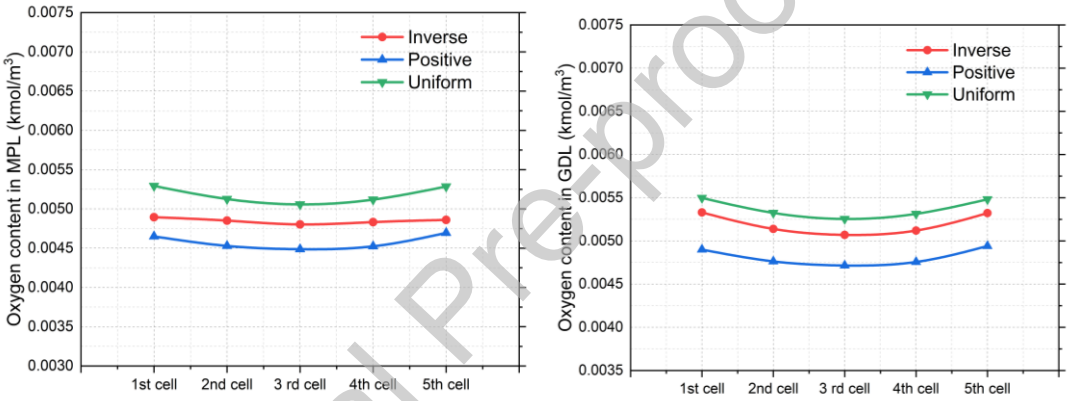

(a) (b)

Figure. 7. Oxygen contents: (a) in cathode MPL; (b) in cathode GDL

3.4 EIS results

In this section, the EIS test is used to verify the mass transport ability of GDM with different hydrophobicity gradients. Corresponding to the inverse, positive, and uniform hydrophobicity gradients in the simulation, the MEAs have been produced with different hydrophobicity gradients in the cathode GDM. The experiment steps and parameters are described in Section 2.3.

The equivalent circuit model is used to fit the result of the EIS test. The equivalent circuit models and the corresponding relationships with EIS are shown in Figure 8. The ohmic resistance R1 is equivalent to ohmic loss, R2 is equivalent to

cathode activation loss which is mainly related to the catalyst, and R3 is mass transfer impedance equivalent to concentration loss in the cathode which can represent the water contents of the MPL and GDL. CPE1 represents the storage of charge at the electrolyte interface of the cathode, and CPE2 represents the quasi-capacitance caused by the uneven diffusion coefficient of the gas in the catalytic layer and the GDM[11],[44]. The result of the EIS test and fitting curve are shown in Figure 9.

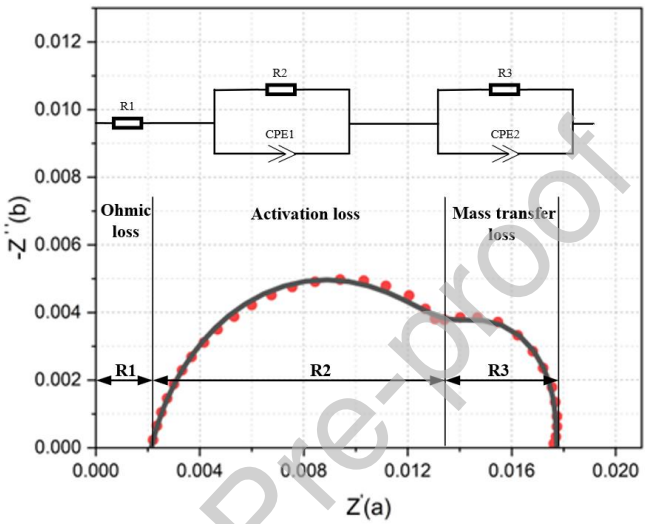

Figure. 8. Equivalent circuit model and corresponding relationship with EIS

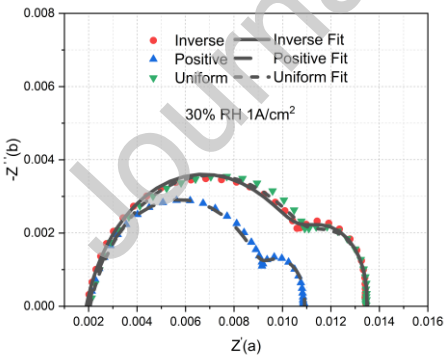

(a)

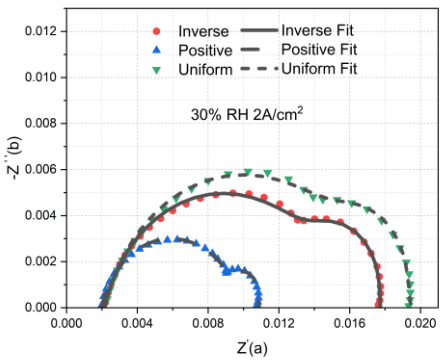

(b)

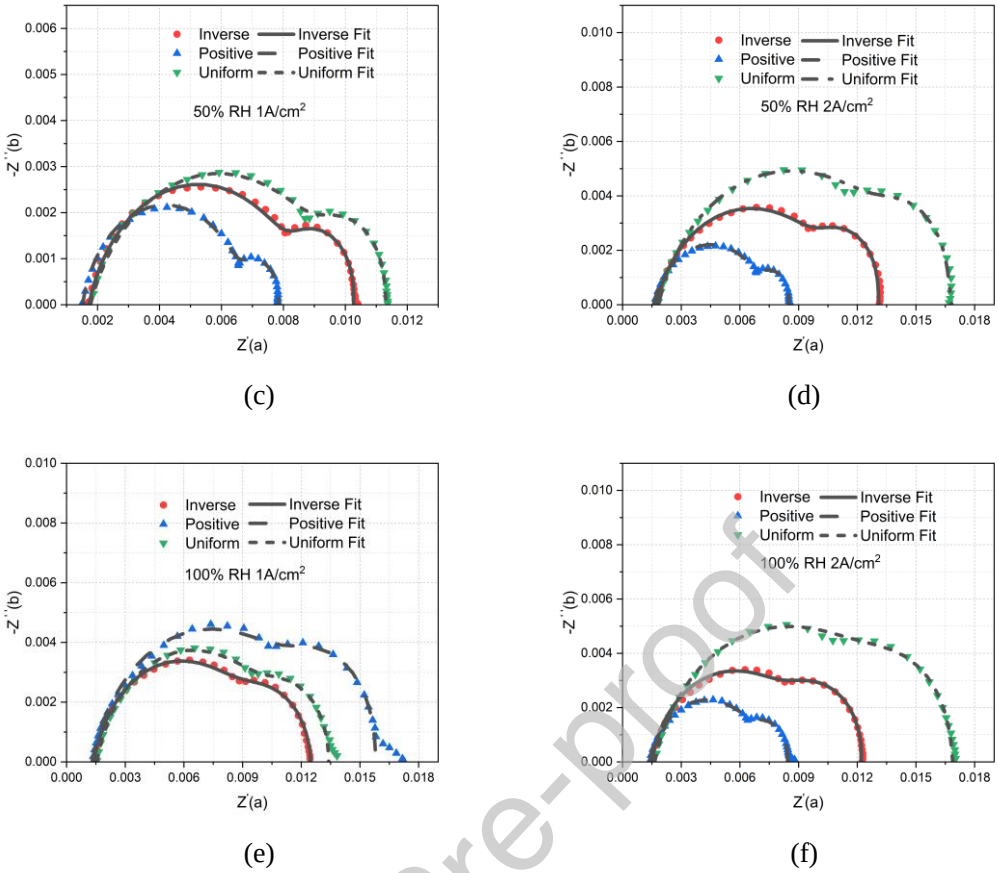

Figure. 9. EIS and fitting curves at different conditions. (a) 30% RH and 1 A cm^{-2}, (b) 30% RH and 2 A cm^{-2}, (c) 50% RH and 1 A cm^{-2}, (d) 50% RH and 2 A cm^{-2}, (e) 100% RH and 1 A cm^{-2}, (f) 100% RH and 2 A cm^{-2}.

In this study, we focus on the water removal ability of MPL and GDL, which can be represented by R3. The comparison of R3 for the fitting curves is shown in Figure 10. From Figure 10, the R3 of the positive gradient is the lowest and that of the inverse gradient is the highest in most cases. The R3 values of the positive gradient show that the positive gradient has a better reaction gas transport ability in cathode GDM. The inverse gradient may have more water in cathode GDM, hindering the transport of reaction gas and leading to the increase of R3. It is noticed that the R3 of the positive gradient is increased and becomes the largest one under 100% RH and 1 A cm^{-2}. However, the R3 of the positive gradient under 100% RH and 1 A cm^{-2} is not much different from others. The reason for R3 of positive gradient increase under 100% RH and 1 A cm^{-2} may be that the water generated under the 2 A cm^{-2} is not completely removed from the interface between the GDL and GC. From the comparison of R3,

we could conclude that the inverse gradient has a weak water removal and oxygen transport ability among the three hydrophobicity gradients, and the positive gradient is the best.

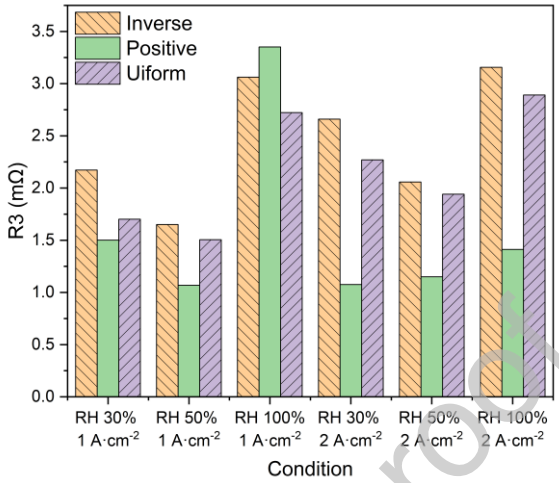

Figure. 10. Comparison of R3 with different hydrophobicity gradients

3.5 Optimization

According to the above analysis, the simulation model has been verified by experiments to predict performance under different hydrophobicity gradients. To obtain a better hydrophobicity gradient in cathode GDM, the optimization for the contact angles of MPL and GDL has been carried out. A single-channel model has been built considering the computational efficiency. The length, height, and width of the single-channel model are based on the 5-cell stack GC. The computational domain of the single-channel model is shown in Figure 11.

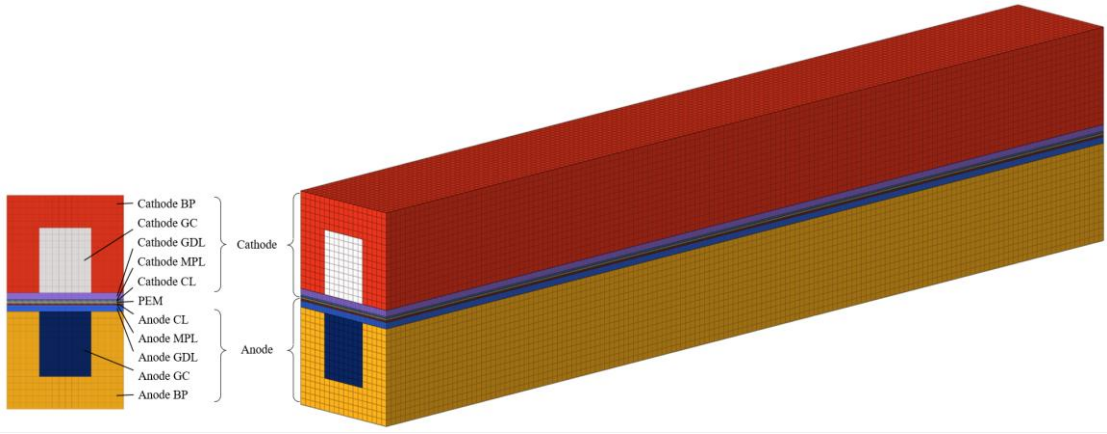

Figure. 11. Computational domain of single-channel model

Both the Matlab and Fluent are used together to optimize the water content in the cathode GDM of PEMFC. Since the genetic algorithm has the characteristics of fast searchability, randomness, being difficult to fall into local optimum, and easy integration with other algorithms[46], the genetic algorithm is selected as the optimization method in the present research. The flow chart of optimization is shown in Figure 12. During the computation process, the Matlab and Fluent interact with the TUI (Text User Interface) command. Step 1 is to run the genetic algorithm for hydrophobicity gradient optimization, while the cathode GDM water content at the 0.65V is set as the objective. Step 2 is to change the value of the contact angles of MPL and GDL to form a different hydrophobicity gradient. Step 3 is to modify the porosity values of MPL and GDL with Eq (11) based on the contact angles from Step 2 considering the coupled effects between the hydrophobicity gradient and the porosity. Step 4 is to change the simulation parameters of Fluent by generating the TUI command and sending the TUI command to Fluent to start the simulation. Step 5 is to get the simulation result from Fluent, and compare the water content of the GDM between the current and last iterations. Steps 1-5 are repeated until the genetic algorithm converges.

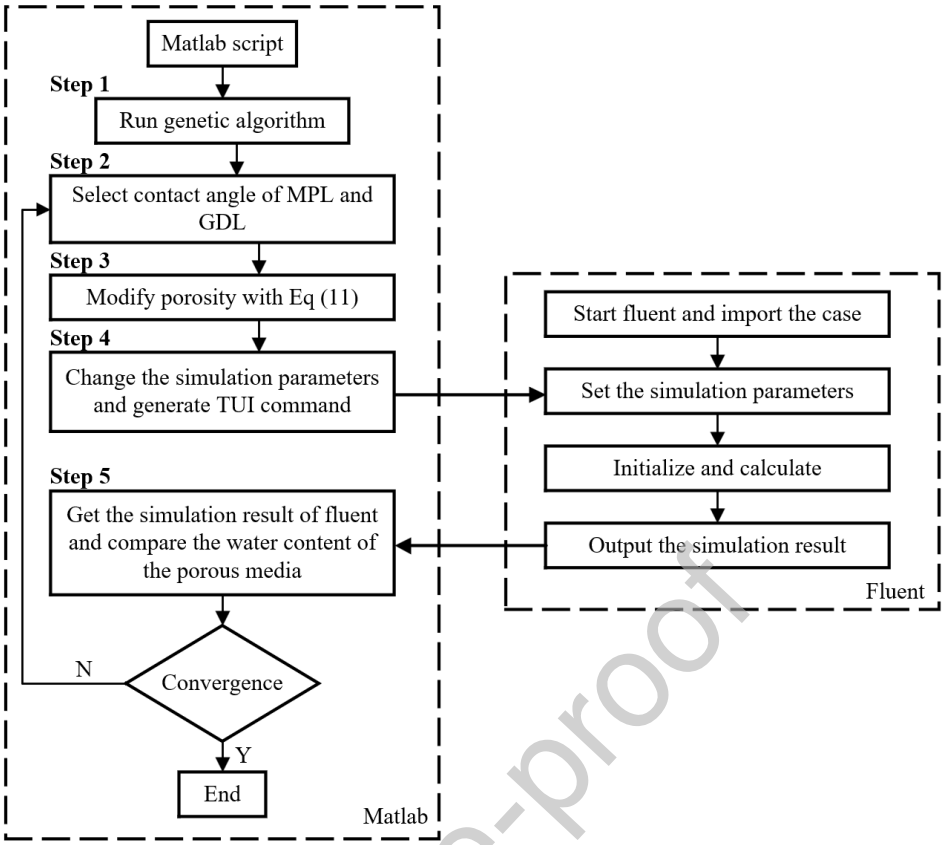

Figure. 12. Flow chart of computation with both the Matlab and the Fluent

The contact angles of MPL and GDL are optimized as 147.9° and 138.6°, respectively. This optimal gradient is applied to the 5-cell stack for further simulations and compared with the positive gradient with angles of 120°-95° at the same current density. Figure 13 shows the concentration distribution and the comparison of oxygen and water on the cathode CL-MPL interface between the optimal and positive gradients. For the oxygen concentration distribution, it is seen that the oxygen distributions in the stack are uniform, and the optimal gradient has a higher oxygen concentration than that with the positive gradient. The water concentration distributions are different in stacks. The water concentrations in the 2^{nd}, 3^{rd}, and 4^{th} cells are higher than those in the 1^{st} and 5^{th} cells. The water concentration of the positive gradient is slightly higher than the concentration at the optimal gradient. To better verify the optimization result, we have calculated the water and oxygen contents in MPL and GDL of positive and optimal gradients, as shown in Table 5. The water contents of the optimal gradients have reduced by 0.67% and 0.42% in MPL and GDL, respectively. The oxygen contents of the optimal gradient have increased

by 12.33% and 11.07% in MPL and GDL, respectively. The optimal gradient shows a better water removal and oxygen transport ability, indicating that the optimal gradient helps to avoid flooding.

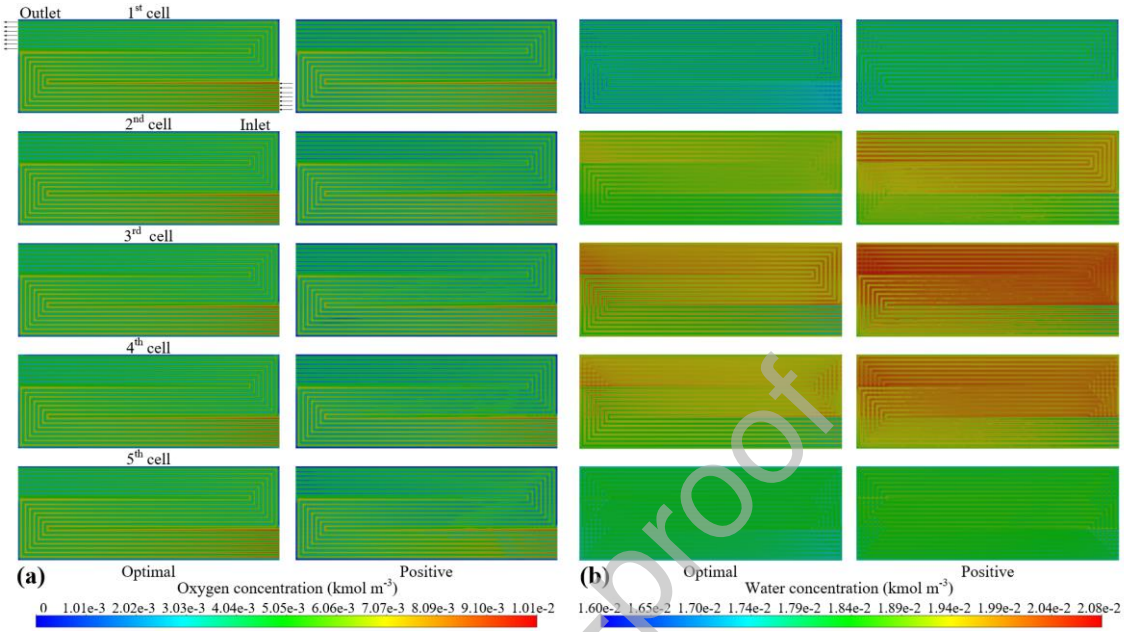

Figure. 13. The concentration distributions of oxygen and water at the cathode CL-MPL interface: (a) oxygen concentration; (b) water concentration.

Table 5. Water and oxygen content comparison between the optimal and positive gradients

Parameters	Gradient	1st cell	2nd cell	3rd cell	4th cell	5th cell
Water content in	Positive	0.01783	0.01928	0.01983	0.01959	0.01837
MPL (kmol m^{-3})	Optimal	0.01769	0.01914	0.01970	0.01947	0.01826
Water content in	Positive	0.01757	0.01901	0.01956	0.01933	0.01814
GDL (kmol m^{-3})	Optimal	0.01750	0.01892	0.01948	0.01926	0.01808
Oxygen content in	Positive	0.004651	0.004530	0.004487	0.004525	0.004695
MPL (kmol m^{-3})	Optimal	0.005310	0.005085	0.005008	0.005052	0.005256
Oxygen content in	Positive	0.004900	0.04763	0.004716	0.004756	0.004941
GDL (kmol m^{-3})	Optimal	0.005521	0.005293	0.005212	0.005256	0.005460

4 Conclusions

In the present research, the contact angles of GDM have been investigated and optimized for water management of PEMFC engine in FCVs, considering the effect of PTEFE treatment on porosity. The main findings can be concluded as follows:

1. With simulations for the 5-cell stack, it is found that GDM with a positive hydrophobicity gradient has better water removal and oxygen transport abilities. Meanwhile, the Eulerian model is used to simulate the droplet behavior in GDM. The droplet has different behaviors at the interface with different hydrophobicity gradient media, leading to the variation of water removal ability. The droplet can easily pass the interface in the positive gradient. EIS test has been conducted for MEAs with different hydrophobicity gradients. The mass transfer impedance of the EIS results has proved that the positive gradient has a better capacity of water removal and oxygen transport.
2. The contact angles for MPL and GDL have been optimized by integrating the CFD simulation model and the genetic algorithm optimization method as 147.9° and 138.6° for MPL and GDL respectively. The coupled relationship between the hydrophobicity gradient and the porosity has been considered and quantified by porosity changes with both the CFD and optimization operations. With the optimal gradient, the water removal and oxygen transport abilities in MPL and GDL of the 5-cell stack have proved to be better than those with the inverse, positive, and uniform gradients. Comparing with the positive gradient (120°-95°), the water contents of the optimal gradients have reduced by 0.67% and 0.42% in MPL and GDL. The oxygen contents of the optimal gradient have increased by 12.33% and 11.07% in MPL and GDL.

Acknowledgement

This research work is supported by the National Natural Science Foundation of China (Nos. 51975196 & 52075159), Virtual Reality Key Application Technology Research (Revealed and Commanded) Project of Jiangxi Province (No. 20213ABC03V01), High Level and High Skill Leading Talent Training Project of Jiangxi Province, the Jiangxi Provincial Natural Science Foundation (20224ACB218002) and the open foundation of Guangxi Key Laboratory of Processing for Non-ferrous Metals and Featured Materials, Guangxi University (No. 2022GXYSOF24).

References

[1] Kandlikar, S. G.; Garofalo, M. L.; Lu, Z., Water management in a PEMFC: Water transport mechanism and material degradation in gas diffusion layers. *Fuel Cells* **2011,** *11* (6), 814-823.

[2] Xu, X.; Li, K.; Liao, Z.; Cao, J.; Wang, R., A closed-loop water management methodology for PEM fuel cell system based on impedance information feedback. *Energies* **2022,** *15* (20).

[3] Yang, Z.; Du, Q.; Jia, Z.; Yang, C.; Jiao, K., Effects of operating conditions on water and heat management by a transient multi-dimensional PEMFC system model. *Energy* **2019,** *183*, 462-476.

[4] Schmittinger, W.; Vahidi, A., A review of the main parameters influencing long-term performance and durability of PEM fuel cells. *Journal of Power Sources* **2008,** *180* (1), 1-14.

[5] Luo, L.; Huang, B.; Cheng, Z.; Jian, Q., Improved water management by alternating air flow directions in a proton exchange membrane fuel cell stack. *Journal of Power Sources* **2020,** *466*.

[6] Liso, V.; Simon Araya, S.; Olesen, A. C.; Nielsen, M. P.; Kær, S. K., Modeling and experimental validation of water mass balance in a PEM fuel cell stack. *International Journal of Hydrogen Energy* **2016,** *41* (4), 3079-3092.

[7] Chen, H.; Xu, S.; Pei, P.; Qu, B.; Zhang, T., Mechanism analysis of starvation in PEMFC based on external characteristics. *International Journal of Hydrogen Energy* **2019,** *44* (11), 5437-5446.

[8] Su, H.; Ye, D.; Cai, Y.; Guo, W., Air starvation of proton exchange membrane fuel cells and its beneficial effects on performance. *Applied Energy* **2022,** *323*.

[9] Wang, L.; Zhang, W.; Wang, T.; Zhu, Y.; Deng, C., Effect of IrO2 on reversal potential for proton exchange membrane fuel cells. *Chinese Journal of Power Sources* **2019,** *43(07)*, 1147-1150+1167.

[10] Pei, P.; Chen, H., Main factors affecting the lifetime of Proton Exchange Membrane fuel cells in vehicle applications: A review. *Applied Energy* **2014,** *125*, 60-75.

[11] Chen, G.; Zhang, G.; Guo, L.; Liu, H., Systematic study on the functions and mechanisms of micro porous layer on water transport in proton exchange membrane fuel cells. *International Journal of Hydrogen Energy* **2016,** *41* (9), 5063-5073.

[12] Chen, Y.; Tian., T.; Wan., Z.; Wu., F.; Tan., J.; Pan., M., Influence of PTFE on water transport in gas diffusion layer of polymer electrolyte membrane fuel cell. *International Journal of Electrochemical Science* **2018**, 3827-3842.

[13] Weng, F.-B.; Hsu, C.-Y.; Su, M.-C., Experimental study of micro-porous layers for PEMFC with gradient hydrophobicity under various humidity conditions. *International Journal of Hydrogen Energy* **2011,** *36* (21), 13708-13714.

[14] Liu, Z.; Zhou, L.; Gao, Y.; Qi, M.; Chen, H.; Hou, M.; Shao, Z., A novel hydrophilic‐modified gas diffusion layer for proton exchange membrane fuel cells operating in low humidification. *International Journal of Energy Research* **2021,** *45* (11), 16874-16883.

[15] Wang, X. L.; Zhang, H. M.; Zhang, J. L.; Xu, H. F.; Tian, Z. Q.; Chen, J.; Zhong, H. X.; Liang, Y. M.; Yi, B. L., Micro-porous layer with composite carbon black for PEM fuel cells. *Electrochimica Acta* **2006,** *51* (23), 4909-4915.

[16] Naito, H.; Ishikawa, K.; Sasabe, T.; Hirai, S.; Tanuma, T., Investigation of effects of hydrophilic micro-porous layer on liquid water behavior by X-ray imaging. *Journal of Power Sources* **2021,** *507*.

[17] Chun, J. H.; Park, K. T.; Jo, D. H.; Lee, J. Y.; Kim, S. G.; Park, S. H.; Lee, E. S.; Jyoung, J.-Y.;

Kim, S. H., Development of a novel hydrophobic/hydrophilic double micro porous layer for use in a cathode gas diffusion layer in PEMFC. *International Journal of Hydrogen Energy* **2011,** *36* (14), 8422-8428.

[18] Hou, S.; Ye, Y.; Liao, S.; Ren, J.; Wang, H.; Yang, P.; Du, K.; Li, J.; Peng, H., Enhanced low-humidity performance in a proton exchange membrane fuel cell by developing a novel hydrophilic gas diffusion layer. *International Journal of Hydrogen Energy* **2020,** *45* (1), 937-944.

[19] Tanuma, T.; Kinoshita, S., Impact of Gas Diffusion Layers (GDLs) on water transport in PEFCs. *Journal of The Electrochemical Society* **2011,** *159* (2), B150-B154.

[20] Ismail, M. S.; Damjanovic, T.; Ingham, D. B.; Pourkashanian, M.; Westwood, A., Effect of polytetrafluoroethylene-treatment and microporous layer-coating on the electrical conductivity of gas diffusion layers used in proton exchange membrane fuel cells. *Journal of Power Sources* **2010,** *195* (9), 2700-2708.

[21] Reshetenko, T. V.; St-Pierre, J.; Artyushkova, K.; Rocheleau, R.; Atanassov, P.; Bender, G.; Ulsh, M., Multianalytical study of the PTFE content local variation of the PEMFC gas diffusion layer. *Journal of The Electrochemical Society* **2013,** *160* (11), F1305-F1315.

[22] Hwang, G. S.; Weber, A. Z., Effective-diffusivity measurement of partially-saturated fuel-cell gas-diffusion layers. *Journal of The Electrochemical Society* **2012,** *159* (11), F683-F692.

[23] Jinuntuya, F.; Kamsanam, W., Effects of Structure and hydrophobic treatment on water transport behaviour in PEM fuel cell gas diffusion layers. *IOP Conference Series: Materials Science and Engineering* **2019,** *501*, 012051.

[24] Kuwertz, R.; Aoun, N.; Turek, T.; Kunz, U., Influence of PTFE content in gas diffusion layers used for gas-phase hydrogen chloride electrolysis with oxygen depolarized cathode. *Journal of The Electrochemical Society* **2016**, *163* (9), F988-F997.

[25] Ding, R.; Zhang, S.; Chen, Y.; Rui, Z.; Hua, K.; Wu, Y.; Li, X.; Duan, X.; Wang, X.; Li, J.; Liu, J., Application of machine learning in optimizing proton exchange membrane fuel cells: a review. *Energy and AI* **2022**, *9*.

[26] Wang, J.; Jiang, H.; Chen, G.; Wang, H.; Lu, L.; Liu, J.; Xing, L., Integration of multi-physics and machine learning-based surrogate modelling approaches for multi-objective optimization of deformed GDL of PEM fuel cells. *Energy and AI* **2023,** *14*.

[27] Zhang, G.; Jiao, K., Three-dimensional multi-phase simulation of PEMFC at high current density utilizing Eulerian-Eulerian model and two-fluid model. *Energy Conversion and Management* **2018,** *176*, 409-421.

[28] Arif, M.; Cheung, S. C. P.; Andrews, J., Influence of hydrophobicity and porosity of the gas diffusion layer on mass transport losses in PEM fuel cells: a simulation study supported by experiments. *Energy & Fuels* **2020,** *34* (10), 13010-13022.

[29] Chen, R.; Qin, Y.; Ma, S.; Du, Q., Numerical simulation of liquid water emerging and transport in the flow channel of PEMFC using the volume of fluid method. *International Journal of Hydrogen Energy* **2020,** *45* (54), 29861-29873.

[30] Ferreira, R. B.; Falcão, D. S.; Oliveira, V. B.; Pinto, A. M. F. R., 1D + 3D two-phase flow numerical model of a proton exchange membrane fuel cell. *Applied Energy* **2017,** *203*, 474-495.

[31] Hou, Y.; Deng, H.; Zamel, N.; Du, Q.; Jiao, K., 3D lattice Boltzmann modeling of droplet motion in PEM fuel cell channel with realistic GDL microstructure and fluid properties. *International Journal of Hydrogen Energy* **2020,** *45* (22), 12476-12488.

[32] Ira, Y.; Bakhshan, Y.; Khorshidimalahmadi, J., Effect of wettability heterogeneity and compression on liquid water transport in gas diffusion layer coated with microporous layer of PEMFC. *International Journal of Hydrogen Energy* **2021,** *46* (33), 17397-17413.

[33] Deng, H.; Hou, Y.; Jiao, K., Lattice Boltzmann simulation of liquid water transport inside and at interface of gas diffusion and micro-porous layers of PEM fuel cells. *International Journal of Heat and Mass Transfer* **2019,** *140*, 1074-1090.

[34] Zhang, H.; Zhan, Z.-g.; Chen, B.; Sui, P.-j.; Pan, M., Anisotropic transport properties of gas diffusion layer based on pore-scale model. *Journal of Jilin University (Engineering and Technology Edition)* **2022,** *52(09)*, 2055-2062.

[35] Niu, Z.; Bao, Z.; Wu, J.; Wang, Y.; Jiao, K., Two-phase flow in the mixed-wettability gas diffusion layer of proton exchange membrane fuel cells. *Applied Energy* **2018,** *232*, 443-450.

[36] Zhang, G.; Yuan, H.; Wang, Y.; Jiao, K., Three-dimensional simulation of a new cooling strategy for proton exchange membrane fuel cell stack using a non-isothermal multiphase model. *Applied Energy* **2019,** *255*.

[37] Wood., D. L.; Rulison., C.; Borup., R. L., Surface properties of PEMFC gas diffusion layers. *Journal of The Electrochemical Society* **2009,** *Volume 157, Number 2*, B195.

[38] Chen, L.; Luan, H.-B.; Tao, W.-Q., Liquid water dynamic behaviors in the GDL and GC of PEMFCS using Lattice Boltzmann Method. *Frontiers in Heat and Mass Transfer* **2010,** *1* (2).

[39] Zhao, X.; Wang, R.; Zhang, Y.; Hao, D.; Yang, Z.; Wu, R., Study on Water transport mechanisms of the PEMFC Based on a visualization platform and water balance model. *International Journal of Chemical Engineering* **2021,** *2021*, 1-12.

[40] Cho, J. I. S.; Neville, T. P.; Trogadas, P.; Bailey, J.; Shearing, P.; Brett, D. J. L.; Coppens, M. O., Capillaries for water management in polymer electrolyte membrane fuel cells. *International Journal of Hydrogen Energy* **2018**, *43* (48), 21949-21958.

[41] Yuan, H.; Dai, H.; Du, R.; Wei, X., Distribution of relaxation times analysis of proton exchange membrane fuel cell electrochemical impedance spectra. *Journal of Mechanical Engineering* **2020,** *56* (22).

[42] Xia, Z.; Chen, H.; Zhang, T.; Pei, P., Effect of channel-rib width ratio and relative humidity on performance of a single serpentine PEMFC based on electrochemical impedance spectroscopy. *International Journal of Hydrogen Energy* **2022,** *47* (26), 13076-13086.

[43] Shao, H.; Qiu, D.; Peng, L.; Yi, P.; Lai, X., In-situ measurement of temperature and humidity distribution in gas channels for commercial-size proton exchange membrane fuel cells. *Journal of Power Sources* **2019,** *412*, 717-724.

[44] Zhang, S.; Dai, H.; Yuan, H.; Ming, P.; Wei, X., Sensibility study on electrochemical impedance of proton exchange membrane fuel cell. *Journal of Mechanical Engineering* **2021,** *57* (14).

[45] Carcadea, E.; Varlam, M.; Ismail, M.; Ingham, D. B.; Marinoiu, A.; Raceanu, M.; Jianu, C.; Patularu, L.; Ion-Ebrasu, D., PEM fuel cell performance improvement through numerical optimization of the parameters of the porous layers. *International Journal of Hydrogen Energy* **2020,** *45* (14), 7968-7980.

[46] Ebrahimi, S.; Ghorbani, B.; Vijayaraghavan, K., Optimization of catalyst distribution along PEMFC channel through a numerical two-phase model and genetic algorithm. *Renewable Energy* **2017,** *113*, 846-854.

Author Biography

Qinwen Yang, Ph.D., Associate Professor, engaged in the research areas of new energy power system design, mechanical design theory and optimal design. She presides over two national level projects, one provincial key projects and several other projects. She has published more than 30 academic papers, including 10 top journal papers and one ESI highly cited papers. She has three invention patents been authorized and four mechanical professional textbooks were issued under her general editorship.

Gang Xiao, Ph.D., Associate Professor, engaged in the research areas of nonline
ar system modeling, optimization and control. He is selected into the 2022 Jiangxi Provincial High-level and High-skilled Leading Talent Training Project and awarded the Jiangxi Provincial Outstanding Youth Fund; He presides over and participates in more than 40 scientific research and education reform projects, and published more than 100 academic papers, of which more than 50 were included in SCI and EI; He also has more than 40 invention patents been authorized and registered 5 computer software copyrights. He has participated in 5 CRRC enterprise standards establishment. Eleven mechanical professional textbooks were issued under his general editorship.

Graphical Abstract

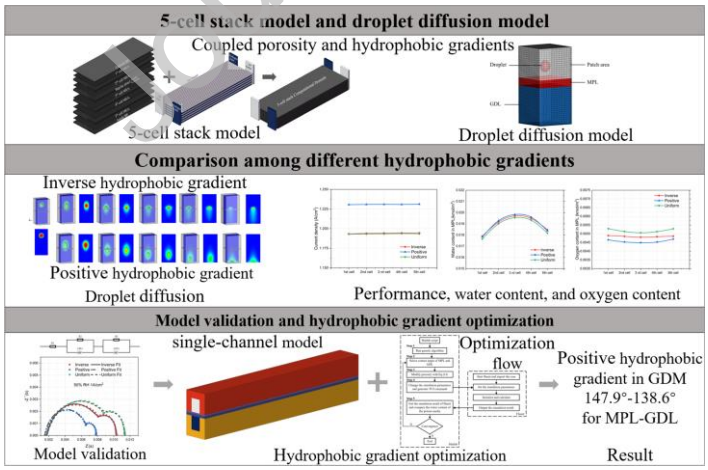

Declaration of Interests

☒ The authors declare that they have no known competing financial interests or personal relationships that could have appeared to influence the work reported in this paper.

☐The authors declare the following financial interests/personal relationships which may be considered as potential competing interests: